Biophysical Journal, Volume 99

Supporting Material

The vesicle trafficking protein Sar1 lowers lipid membrane rigidity

Edward I. Settles, Andrew F. Loftus, Alesia N. McKeown, and Raghuveer Parthasarathy

Supporting Information for

The vesicle trafficking protein Sar1 lowers lipid membrane rigidity

Edward I. Settles, Andrew F. Loftus, Alesia N. McKeown, Raghuveer Parthasarathy

Contents

SI Text: Derivation of force and rigidity relations for membrane tethers

General principles of membrane mechanics as well as the limitations of simple continuum models are described, for example, in (S1-S6). Aspects of tether mechanics are discussed in Refs. (S7-S10).

The bending energy per unit area of a membrane, ε, is a function of geometric and material parameters (1):

$$\varepsilon = \left[\frac{\kappa}{2} \left(R_1^{-1} + R_2^{-1} - 2c_0 \right)^2 \right] + \kappa_G R_1^{-1} R_2^{-1},$$

where R_1 and R_2 are the principle radii of curvature, c_0 is the spontaneous curvature (which gives the curvature at which the bracketed term is minimal), κ is the bending modulus (i.e. the rigidity), and κ_G is the Gaussian curvature modulus.

Membrane inclusions, such as bound or inserted proteins, can change the membrane rigidity directly by altering κ (e.g. by thinning the membrane or altering lipid packing) (S11-13), or indirectly by coupling to the local curvature and reducing the effective rigidity with respect to deformations (S4). The interaction between the inclusions and the membrane can be accounted for by additional energetic terms:

$$\varepsilon_{int} = -\Lambda \phi c + \frac{b}{2} |\nabla \phi|^2 + g(\phi),$$

where ϕ is the density of inclusions, Λ is a coupling constant, and $c = R_1^{-1} + R_2^{-1}$ is the total curvature. The latter two terms describe the interactions of the intercalated particles with themselves. In general $g(\phi)$ is not known; particular forms of $g(\phi)$ are considered, for example, in Refs. (S4) and (S14). As detailed below, κ can be determined in tether-based experiments independent of the form of $g(\phi)$.

Membrane Tethers

We consider a cylindrical membrane tether of radius *R* and length *L*; i.e. $R_1 = R$ and $R_2 = \infty$. The total mechanical energy, *E*, is the sum of several terms: (*i*) the bending energy integrated over the cylinder

area; (*ii*) ε_{int} integrated over the cylinder area; (*iii*) the elastic energy given by the product of the membrane tension, σ, and the cylinder area; and (*iv*) the mechanical work given by the product of the force of extension, f, and *L*:

$$E = \left[\frac{\kappa}{2}\left(R^{-1} - 2c_0 \right)^2 - \Lambda\phi R^{-1} + \frac{b}{2}\left|\nabla\phi\right|^2 + g(\phi) + \sigma \right] 2\pi RL - fL \ . \qquad \textbf{(Eq. 1)}$$

Neglecting non-uniformities in ϕ, this becomes:

$$E = \left[\frac{\kappa}{2}\left(R^{-1} - 2c_0 \right)^2 - \Lambda\phi R^{-1} + g(\phi) + \sigma \right] 2\pi RL - fL \ . \qquad \textbf{(Eq. 2)}$$

The tether adopts the minimal energy configuration such that $\frac{\partial E}{\partial R} = 0$ and $\frac{\partial E}{\partial L} = 0$.

From the first condition, $\sigma + g(\phi) = \frac{\kappa}{2}\left(R^{-2} - 4c_0^2 \right)$. **(Eq. 3)**

From the second, $f = \left[\frac{\kappa}{2}\left(R^{-1} - 2c_0 \right)^2 - \Lambda\phi R^{-1} + \sigma + g(\phi) \right] 2\pi R$ **(Eq. 4)**

Rigidity

Equations (3) and (4) can be combined to eliminate $\sigma + g(\phi)$:

$$\frac{fR}{2\pi} = \kappa\left[1 - \left(2c_0 + \frac{\Lambda\phi}{\kappa} \right) R \right] \qquad \textbf{(Eq. 5)}$$

Several aspects of Equation 5 are worth noting. First, the coupling between the inclusions and the local curvature changes the effective spontaneous curvature; i.e. $c_0 \to c_0 + \Lambda\phi/(2\kappa)$, as in Ref. (S4). (Our expression for the change in the effective spontaneous curvature differs by a factor of two from the general expression in Ref. (S4) because of the one-dimensional tether curvature considered here.) Second, the (unknown) self-interaction among the inclusions drops out of the derivation. Third, for a symmetric lipid bilayer membrane, as in our experiments, the bare spontaneous curvature $c_0 = 0$. Incorporating this, and explicitly writing the possible direct inclusion-dependence of κ as $\kappa(\phi)$,

$$\frac{fR}{2\pi} = \kappa(\phi) - \Lambda\phi R \qquad \textbf{(Eq. 6)}$$

The functional relationship between the measurable force and radius values reveals κ and $\Lambda\phi$. Note that in the absence of coupling between the inclusions and the curvature ($\Lambda = 0$), $fR = 2\pi\kappa$, motivating our expression for the bending modulus $\kappa_{\Lambda=0} = fR\left(2\pi\right)^{-1}$. We caution against thinking of $fR\left(2\pi\right)^{-1}$ as an "effective rigidity" of the membrane from which one can predict arbitrary membrane properties; general statements about effective rigidity of membranes with curvature-coupled proteins are intrinsically dependent on the form of the protein self-interaction, $g(\phi)$ (S4).

Tension

Equations (3) and (4) can be combined to eliminate κ:

$$\sigma + g(\phi) = \left(\frac{R^{-2} - 4c_0^2}{R^{-2} - 4c_0 R^{-1}} \right) \left(\frac{f}{4\pi R} + \frac{\Lambda \phi}{2R} \right) \qquad \textbf{(Eq. 7)}$$

Again using $c_0 = 0$, this simplifies to

$$\sigma_{\text{eff}} \equiv \sigma + g(\phi) = \left(\frac{f}{4\pi R} + \frac{\Lambda \phi}{2R} \right), \qquad \textbf{(Eq. 8)}$$

Where we have defined σ_{eff} as an effective tension that combines the (indistinguishable) bilayer tension and the self-interaction of the inclusions. If $\Lambda = 0$, $\sigma_{\Lambda=0} = \frac{f}{4\pi R}$.

References

S1. Helfrich, W. (1973) Elastic properties of lipid bilayers: theory and possible experiments. *Z. Naturforsch.* **28c**, 693-703.

S2. Lipowsky, R. & Sackmann, E. (1995) *Structure and Dynamics of Membranes, Vol. 1* (Elsevier, New York).

S3. Safran, S. A. (2003) *Statistical Thermodynamics of Surfaces, Interfaces, and Membranes* (Westview Press, Boulder, CO).

S4. Leibler, S. (1986) Curvature instability in membranes. *J. Phys.* **47**, 507-516.

S5. Parthasarathy, R. & Groves, J. T. (2007) Curvature and spatial organization in biological membranes. *Soft Matter* **3**, 24-33.

S6. Zimmerberg, J. & Kozlov, M. M. (2006) How proteins produce cellular membrane curvature. *Nat. Rev. Mol. Cell Biol.* **7**, 9-19.

S7. Waugh, R. E. & Hochmuth, R. M. (1987) Mechanical equilibrium of thick, hollow, liquid membrane cylinders. *Biophys. J.* **52**, 391-400.

S8. Dai, J. & Sheetz, M. P. (1995) Mechanical properties of neuronal growth cone membranes studied by tether formation with laser optical tweezers. *Biophys. J.* **68**, 988-996.

S9. Derenyi, I., Julicher, F., & Prost, J. (2002) Formation and interaction of membrane tubes. *Phys. Rev. Lett.* **88**, 238101.

S10. Powers, T. R., Huber, G., & Goldstein, R. E. (2002) Fluid-membrane tethers: minimal surfaces and elastic boundary layers. *Phys. Rev. E* **65**, 041901.

S11. Huang, H. W. (1995) Elasticity of lipid bilayer interacting with amphiphilic helical peptides. *J. Phys. II* **5**, 1427-1431.

S12. Huang, H. W. (2006) Molecular mechanism of antimicrobial peptides: the origin of cooperativity. *Biochim Biophys Acta* **1758**, 1292-302.

S13. Pan, J., Tieleman, D. P., Nagle, J. F., Kucerka, N., & Tristram-Nagle, S. (2009) Alamethicin in lipid bilayers: combined use of X-ray scattering and MD simulations. *Biochim Biophys Acta* **1788**, 1387-97.

S14. Bouvrais, H., Meleard, P., Pott, T., Jensen, K. J., Brask, J. et al (2008) Softening of POPC membranes by magainin. *Biophys Chem* **137**, 7-12.

SI Methods

Lipid composition. Lipid membranes were composed of the "Major Mix" mixture as in Ref. 14, modified to include fluorescent probes and biotinylated lipids: 51.5 mol% DOPC (1,2-dioleoyl-sn-glycero-3-phosphocholine), 23.0 mol% DOPE (1,2-di-(9Z-octadecenoyl)-*sn*-glycero-3-phosphoethanolamine), 11.0 mol% PI (L-α-phosphatidylinositol, from Soy), 8.0 mol% DOPS (1,2-diacyl-sn-glycero-3-phosphoserine), 5.0 mol% DOPA (1,2-di-(9Z-octadecenoyl)- *sn*-glycero-3-phosphate), 0.5 mol% Texas Red DHPE (Texas Red 1,2-dihexadecanoyl-sn-glycero-3-phosphoethanolamine), and 1.0 mol% biotinyl-cap-PE (1,2-dihexadecanoyl- *sn*-glycero-3-phosphoethanolamine-N-(cap biotinyl)). For experiments involving hexahistidine-terminated Δ23-Sar1, the membrane included 5 mol% nickel-chelating lipids (DOGS-NTA-Ni, 1,2-di-(9Z-octadecenoyl)-*sn*-glycero-3- [(N-(5-amino-1-carboxypentyl) iminodiacetic acid)succinyl] (nickel salt)), with other lipid fractions proportionally rescaled. All lipids were purchased from Avanti Polar Lipids, except Texas Red DHPE, which was purchased from Invitrogen.

Sar1 expression. Protein expression was performed with a PTY40 expression vector (a pGEX-2T backbone (GE Healthcare) with inserted GST-Sar1p strain RSB245410 or a hexahistidine-Δ23Sar1p insert (47)) in BL21 bacterial expression cells. Proteins were expressed and purified using protocols modified from Ref. (15). In brief, cells were grown in 1L 2xYT broth to an OD600 = 0.2-0.3 at 37 °C. Further growth to an OD600 = 0.7-0.8 at 25 °C was then induced with 0.1 mM IPTG for 1h. Cells were pelleted at 5000 rpm in a Ka9.1 Rotor (Kompsin) for 25 minutes at 5000 rpm and suspended in 20mL of TBST (50mM Tris, 150mM NaCl, 0.1 % Tween-20, pH= 7.4) with the addition of 0.5 mL of a 40mg/mL lysosyme solution on ice for 20 minutes. TX-100 was then added to 1% to the suspension. The cell suspension was then sonicated with a Sonic Dismembrator Model 500 (Fischer Scientific) with pulses of 30 s each, 3 times. The suspension was centrifuged at 15000 rpm in a JA-20 (Beckman) rotor for 20m with the supernatant being transferred to a 50mL Falcon tube. 8ml of a 50% Glutathione Sepharose 4B slurry (GE Healthcare) were washed in TBST 3 times and the beads were transferred to the supernatant tube. The supernatant slurry was incubated for 1h at 4 °C with slow rotation and spun down at 5000 rpm for 5m in a JA-20 with the supernatant being poured off. The beads were then washed subsequently 3 times in TBST, 2 times in TBS (50mM Tris, 150mM NaCl, pH = 7.4), and once in TCB (50mM Tris, 250mM KoAc, 5mM CaCl2, pH= 8.0) each time being spun down at 5000 rpm for 5m in a JA-20 rotor. The beads were transferred to a 10cc miniprep column and incubated with thrombin (4U) for 90min. The protein was then eluted with TCB and buffer exchanged using a PD-10 column with HKM (20mM Hepes, 160mM KoAc, 1mM MgCl2, pH=7.0). The collected fractions were then stored at -80 °C. For the small fraction of experiments involving visualization of Sar1p, proteins were labelled at primary amines with Alexa Fluor 488 fluorophores (Alexa Fluor 488 Microscale Protein Labeling Kit, Invitrogen). For control experiments on the mechanical influence of a hexahistidine tag, synthetic fluorescein-conjugated his_6 was purchased from Biomatik. (The fluorescein enabled verification of membrane binding.)

Sar1 helix peptide. The fluorescein-conjugated peptide corresponding to the N-terminal alpha-helical domain of Sar1p was purchased from Biomatik (sequence from N to C: MAGWDIFGWFRDVLASLGLWNKH, with N-terminal FITC). The addition of 5% dimethylsulfoxide (DMSO) to the buffer was required for peptide solubility

Sample preparation. Approximately 5 μg of lipids dissolved in chloroform were deposited onto chambered glass coverslips. The solvent was evaporated in a vacuum desiccator for 5m after which the lipids were hydrated with 0.2-0.5 ml HKM buffer (20 mM Hepes-KOH, pH 6.8, 160 mM potassium acetate, 1 mM $MgCl_2$), yielding multilayered membrane stacks. These stacks were approximately 1-2 mm in extent and the coverslip chambers were 18mm wide, allowing ample room for the extension of tethers beyond the stack edges. For experiments with 1X (undiluted) HKM, bovine serum albumin (BSA) was adsorbed to the glass prior to lipid deposition in order to prevent van der Waals adhesion of microspheres; BSA was incubated at 1 mg/ml for several hours, followed by repeated washing. Sar1p or Δ23-Sar1, 100 μM GMPPNP (Sigma-Aldrich) and 4 mM EDTA were incubated together in an Eppendorf tube for 5m, after which they were added to the chamber containing membranes and buffer. Approximately five minutes after the addition of protein, a few microliters of a suspension of 4.8 μm diameter streptavidin-coated silica microspheres (Bangs Laboratories) were added to the chamber. The microspheres gravitationally settled and bound to the membranes.

Activation of Sar1 (binding of GMPPNP) was verified by separate experiments measuring the fluorescence emission of the tryptophan residue (Trp 84) located in the switch region of Sar1p, which serves as an indicator of protein conformation (48; 49). Activation was found to require the presence of membranes, as in previous studies of G-proteins (49). Data demonstrating protein activation in the presence of nucleotide, membrane, and buffer are shown in Figure S6, provided as Supporting Information. Tryptophan fluorescence emission was measured over 330-350 nm with excitation at 280 nm.

Low ionic strength (0.05X HKM) was found not to significantly inhibit Sar1-membrane binding, assessed by fluorescence microscopy of fluorophore-conjugated Sar1.

Δ23-Sar1p-GMPPNP bound to membranes containing 5 mol% DOGS-NTA-Ni at protein surface densities approximately 2x higher than wild type Sar1p-GMPPNP, as assessed by fluorescence imaging using labeled proteins. Both wild type Sar1p and Δ23-Sar1p proteins were labeled using the same labeling chemistry, noted above, and incubated with multilayered membranes, as above. Immediately after exchanging the buffer to remove unbound protein, fluorescence images of the bound protein and of fluorescent lipid probes were taken. The background-subtracted protein fluorescence intensities were normalized by the lipid fluorescence intensities to account for any changes in illumination intensity and compared to determine relative protein densities.

Optical trapping and particle tracking. Microspheres were trapped with a home-built optical trap setup using a 671 nm, 120 mW diode laser (Meshtel RS71-100PS) focused through a Nikon 60X NA=1.25 oil-immersion objective lens. The laser propagation axis is perpendicular to the glass coverslip plane. Because the membrane stacks are multilayered, their exposed surfaces are not planar, permitting tether pulling parallel to the glass. Membrane-bound microspheres were pulled parallel to the coverslip, drawing out tethers beyond the finite extent of the multilayered stacks so that the tethers were clearly visible against membrane-free regions of the coverslip; note also that the tether base is necessarily fixed at the stack edge. Microsphere images were captured with bright-field microscopy using a Cooke pco.1200 camera at 100 frames per second. Particle positions were determined using home-built tracking software that employs well-established algorithms (50; 51) with approximately 10 nm precision. As noted in the main text, mechanical properties are determined from analysis of the initial period of constant-velocity (linear) retraction. During this period, we observe no indication of changes in the attachment point between the tether and the bulk membrane reservoir or any other signatures of varying mechanical character.

Drag coefficient. The drag coefficient, b, is determined independently for each tethered microsphere following the general technique described in Ref. (30). The microsphere position (x) is well-described by a constant velocity (v) retraction together with random (Brownian) motion about this linear drift. The probability distribution of step sizes (Δx) between frames separated in time by Δt therefore follows a Gaussian form:

$$P\left(\Delta x\right) = \left(2\pi\sigma^2\right)^{-1/2} \exp\left[-\left(\Delta x - \left\langle \Delta x \right\rangle\right)^2 / \left(2\sigma^2\right)\right]$$

where the mean step size $\left\langle \Delta x \right\rangle = v\,\Delta t$ and the width, σ, is related to b via the Einstein- Smoluchowski relation: $\sigma^2 = 2k_B T\left(\Delta t\right) b^{-1}$, where k_B is Boltzmann's constant and T is the absolute temperature. Analyzing $P\left(\Delta x\right)$ therefore reveals the drag coefficient. Notably, this approach determines b for the tether-plus-microsphere system independent of assumptions about the nature of the dissipation in the system.

Tether images and radii. Fluorescence images of membrane tethers were captured with a Hamamatsu ORCA-ER CCD camera. Tether radii were determined from Texas Red DHPE fluorescence images by measuring the intensity along lines perpendicular to the tether axis, averaged over approximately 1 μm along the tether length. We estimated the uncertainty in optical determination of the tether width by calculating the intensity profiles of ideal tethers, convolving with the microscope point spread function, and comparing the resulting profiles with the observed data. Even for the narrowest tethers (R = 200-300 nm, 7% of the tethers) the correction to the radius values associated with diffraction-limited resolution was at most 10%, and hence is negligible compared to the statistical scatter. For tethers of radii over 300 nm (93% of the data), the radius correction due to diffraction is less than 1%. Peristaltic fluctuations of tethers (Schneider, M. B., Jenkins, J. T., & Webb, W. W. (1984) Thermal fluctuations of large cylindrical phospholipid vesicles. *Biophys. J.* **45**, 891-899), i.e. wiggles from the equilibrium center of mass configuration, are slower by over two orders of magnitude than the exposure times used in fluorescence imaging, and hence do not hinder determination of tether radii.

Table 1: $\kappa_{\Delta=0}$ values (plotted in Figure 2A)

Buffer: 0.05× HKM

[Sar1p] (μg/ml)	Number of tethers examined	$\kappa_{\Delta=0}$ (10^{-20} J)
0	31	5.2 ± 0.3
0.8	19	4.9 ± 0.4
8	34	5.1 ± 0.4
80	33	4.0 ± 0.4
200	6	2.0 ± 0.2

Buffer: 1× HKM

[Sar1p] (μg/ml)	Number of tethers examined	$\kappa_{\Delta=0}$ (10^{-20} J)
0	9	4.3 ± 0.3
0.8	26	3.5 ± 0.4
8	12	2.8 ± 0.2
80	11	2.1 ± 0.2
200	6	0.7 ± 0.1

The stated uncertainties are the standard errors of the means.

Legend for Movie 1

A movie of spontaneous membrane disintegration following the addition of addition of Sar1p-GMPPNP at 400 μg/ml. Width: 43 microns. Duration: 14.5 seconds. The images are of Texas Red DHPE fluorescence, as in Figures 1B and 2B.

Supporting Figure Captions

Figure S1. The measured drag coefficient, *b*, as a function of Sar1p-GMPPNP concentration. The dashed gray line indicates the Stokes drag of a 4.8 μm diameter sphere in an infinite extent of water.

Figure S2. $\kappa_{\Lambda=0}$ as a function of Sar1p-GMPPNP concentration for experiments at 1X HKM buffer. Circles: Values derived from all tethers, as in Figure 2A. Triangles: Values derived from subsets of the tethers with radii smaller than and larger than the median (0.4 μm). Error bars indicate the standard errors of the means.

Figure S3. $\Lambda\phi$, a measure of the coupling between Sar1 and local curvature, as a function of Sar1p-GMPPNP concentration. Negative values indicate an energetic preference for concave curvature. At [Sar1p] = 0, $\Lambda\phi = 0$, as expected. For comparison, 80 μg/ml Δ23-Sar1p in 0.05X HKM shows $\Lambda\phi = (-9.9 \pm 1.1) \times 10^{-20}$ J/μm. The values and uncertainties are determined from a linear fit of fR vs. R (Equation 1).

Figure S4. $\kappa_{\Lambda=0}$ for full-length Sar1p (as in Figure 2A) and a peptide corresponding to the 23 amino acid Sar1p terminal helix domain, in 0.05× HKM buffer. 5% DMSO is required for peptide solubility, and in itself lowers bilayer rigidity.

Figure S5. The effective membrane tension, $\sigma_{\Lambda=0}$, as a function of Sar1p-GMPPNP concentration.

Figure S6. Tryptophan fluorescence emission and Sar1p activation. As described in Methods, the fluorescence of the tryptophan residue in the G-protein switch region of Sar1p and similar proteins serves as an indicator of conformation; fluorescence emission is increased in the GTP-bound state. In the absence of lipids, addition of nucleotide (bar 3) does not lead to enhanced fluorescence, but rather a drop due to UV absorption by the nucleotide. With the addition of membranes (multilamellar suspensions as in the tether assays) fluorescence is strongly enhanced, indicating nucleotide uptake (bar 4). The Sar1p concentration is 40 μg/ml; the buffer and the concentrations of all other reagents are the same as in the tether pulling assays. The absence of EDTA, which chelates Mg^{2+} present in the buffer, does not significantly alter Sar1p activation (bar 5). Mg^{2+} inhibits nucleotide release and hence slows nucleotide exchange rates; in our experiments, Sar1p is not pre-loaded with nucleotide, likely explaining the lack of significance of EDTA.

Supporting Figures

Figure S1

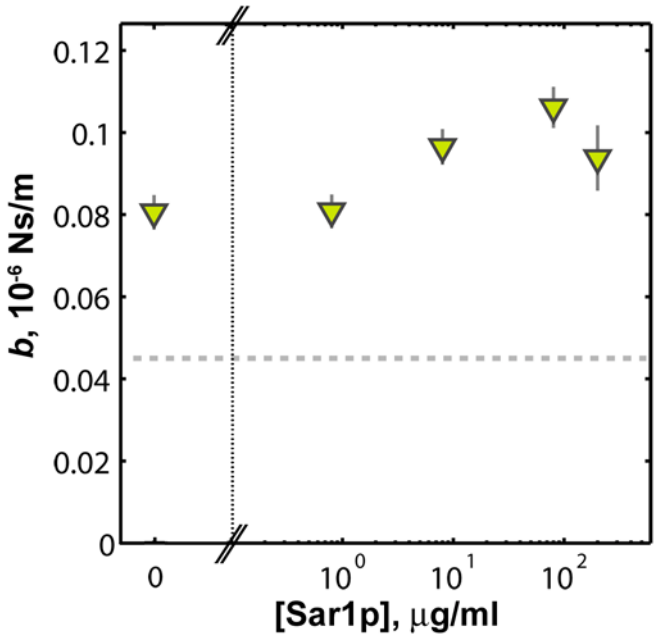

Figure S2

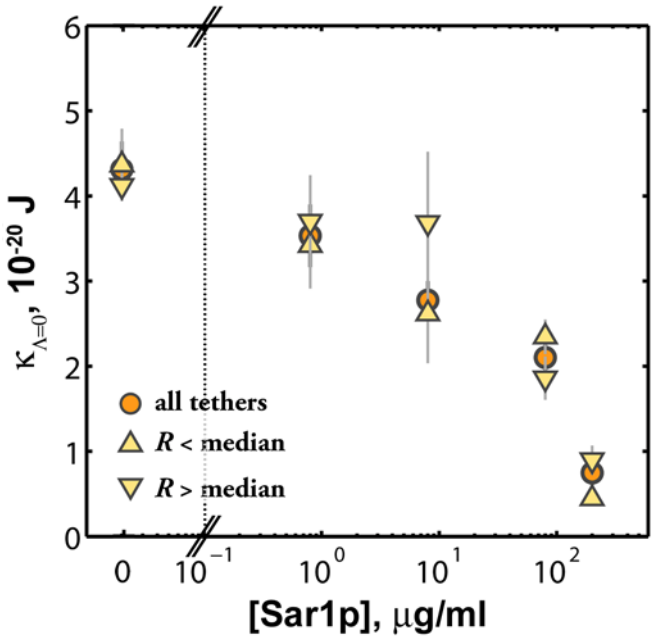

Figure S3

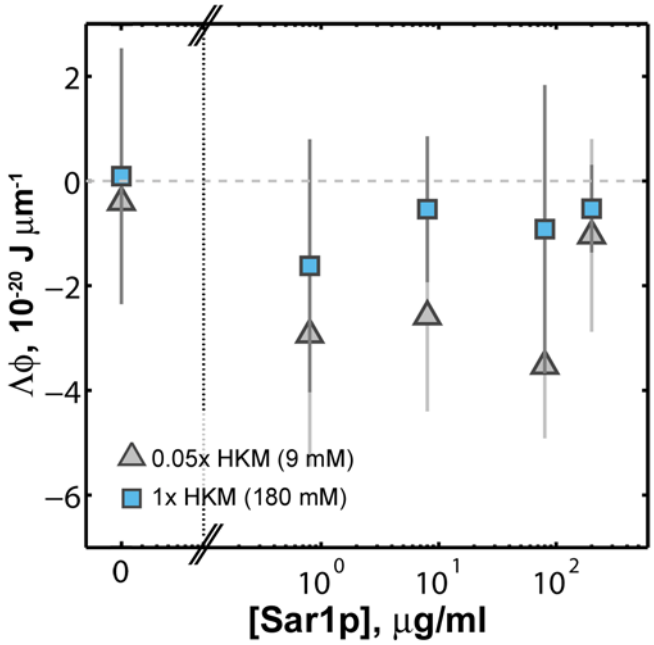
2
0
−2
−4
−6
Δϕ, 10-20 J μm-1
0.05x HKM (9 mM)
1x HKM (180 mM)
0
10 0
10 1
10 2
[Sar1p], μg/ml

Figure S4

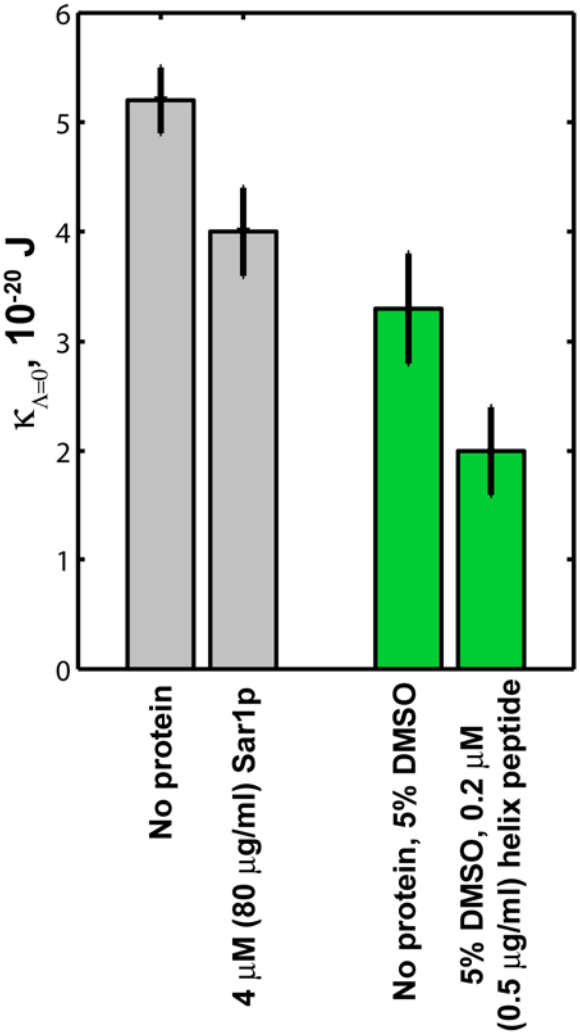
$\kappa_{\Lambda=0}$, 10^{-20} J
0
1
2
3
4
5
6
No protein
4 μM (80 μg/ml) Sar1p
No protein, 5% DMSO
5% DMSO, 0.2 μM
(0.5 μg/ml) helix peptide

Figure S5

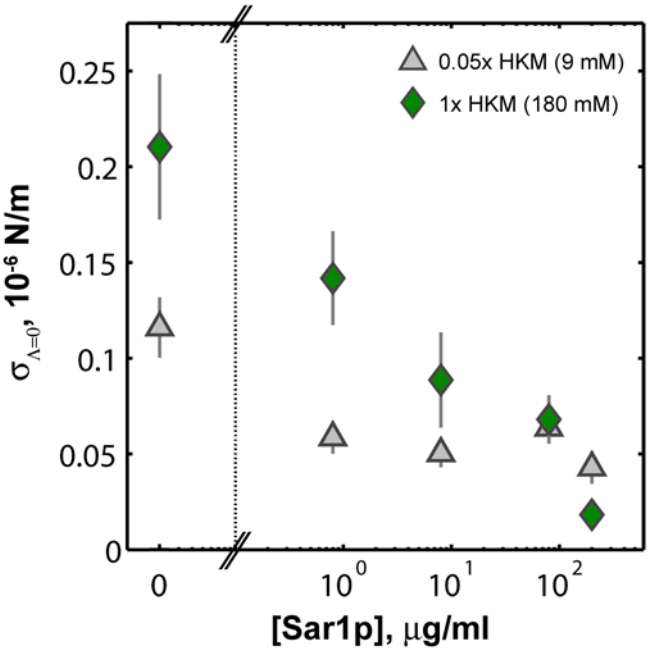

Figure S6